Neutron diffraction studies of magnetic structures of $R_2Ni_3Si_5$ (R=Tb, Dy, Ho) compounds

# Neutron diffraction studies of magnetic structures of $R_2Ni_3Si_5$ (R = Tb, Dy, Ho) compounds*

A Szytuła†, M Kolenda†, E Ressouche‡ and W Sikora§

† Institute of Physics, Jagellonian University, 30-059 Kraków, Reymonta 4, Poland
‡ Départment de Recherche Fondamentale sur la Matiére Condensée, SPS-MDN, CEA Grenoble, 17 rue des Martyrs, 38054 Grenoble Cédex 9, France
§ Department of Physics and Nuclear Techniques, Academy of Mining and Metallurgy, Reymonta 19, 30-059 Kraków, Poland

**Abstract.** Neutron diffraction studies of polycrystalline $R_2Ni_3Si_5$ (R = Tb, Dy, and Ho) inter-metallic compounds with the orthorhombic $U_2Co_3Si_5$-type crystal structure indicate different magnetic structures. For R = Tb, below $T_\tau = 13$ K, a collinear antiferromagnetic structure with a magnetic unit cell equal to the crystal one is observed. In the temperature region between $T_\tau = 13$ K and $T_N = 19.5$ K, it becomes sine modulated with a wavevector $k = (0, 1.0, 0.206(1))$. In both phases the magnetic moments are parallel to the $c$-axis. $Dy_2Ni_3Si_5$ has an incommensurate sine-modulated structure with the wavevectors $k = (0, 0, 0.330(1))$ at $T = 2$ K and $k = (0, 0.159(8), 0.356(2))$ at $T = 5.5$ K. $Ho_2Ni_3Si_5$ at $T = 2$ K also has a sine-modulated structure with $k = (0, 0, 0.2855(9))$. This structure does not change up to the Néel temperature 7.2 K.

The magnetic structures determined have been confirmed by symmetry analysis.

## 1. Introduction

The lanthanide–transition metal silicides form intermetallics with different compositions. They, especially the $R_2T_3Si_5$ compounds, have been intensively investigated because of their interesting magnetic properties [1]. About fifty $R_2T_3Si_5$ compounds have been reported on in the literature. They crystallize in either the orthorhombic $U_2Co_3Si_5$-type structure or the tetragonal $Sc_2Fe_3Si_5$-type structure [2]. The first structure appears when T is Co, Ni, or Rh, and the second one when T is Mn, Ru, Os, or Fe. The magnetic data reported for $R_2Ni_3Si_5$ compounds (R = Pr, Nd, Sm, Gd, Tb, Dy, and Ho) indicate a magnetic ordering below $T_N = 8.5$, 9.5, 11.0, 15.0 19.5, 9.5, and 6.0 K, respectively [3–5]. $Tb_2Ni_3Si_5$ shows two distinct magnetic transitions at $T_N = 19.5$ K and $T_\tau = 12$ K [5].

In this paper the results of the neutron diffraction investigations of three $R_2Ni_3Si_5$ (R = Tb, Dy, and Ho) compounds are presented.

## 2. Experimental details

The $R_2Ni_3Si_5$ (R = Tb, Dy, and Ho) samples were prepared by a standard arc-melting technique. They were vacuum annealed at 1100 °C for one day, and at 1000 °C for seven days, and then cooled down slowly to room temperature. The x-ray powder diffraction

---

* Dedicated to Professor Wojciech Suski on the occasion of his 60th birthday.

**6651**

patterns of the resulting polycrystalline samples were measured using Co K$\alpha$ radiation. The room temperature powder patterns for all three compounds show that the samples exhibit the orthorhombic $U_2Co_3Si_5$ type of crystal structure (space group *Ibam*) [6] with small admixtures of other unidentified phases.

The neutron diffraction measurements of these compounds were performed in the 35 MW Siloé reactor at Grenoble using a multidetector system. Diffraction diagrams were constructed at different temperatures between 2.0 and 25 K using a neutron wavelength $\lambda = 2.486$ Å. The neutron data were analysed by means of the Rietveld-type FULLPROF program [7]. The nuclear scattering lengths and form factors for $R^{3+}$ ions were taken from references [8] and [9], respectively.

## 3. Results

### 3.1. Crystal structure

The nuclear Bragg peaks observed at a temperature above $T_N$ were indexed in terms of an orthorhombic cell. The positions occupied by the atoms in the *Ibam* space group are given in table 1.

**Table 1.** The positions occupied by the atoms in the *Ibam* space group.

| R | in 8j | $x_R$ | $y_R$ | 0 |
|---|---|---|---|---|
| Ni(1) | in 8j | $x_{Ni1}$ | $y_{Ni1}$ | 0 |
| Ni(2) | in 4b | 0.5 | 0 | 0.25 |
| Si(1) | in 8j | $x_{Si1}$ | $y_{Si1}$ | 0 |
| Si(2) | in 8g | 0 | $y_{Si2}$ | 0.25 |
| Si(3) | in 4a | 0 | 0 | 0.25 |

**Table 2.** Crystal data for $R_2Ni_3Si_5$ (R = Tb, Dy, Ho) and $Y_2Ni_3Si_5$.

| Compound | $Tb_2Ni_3Si_5$ | $Dy_2Ni_3Si_5$ | $Ho_2Ni_3Si_5$ | $Y_2Ni_3Si_5$ [10] |
|---|---|---|---|---|
| $a$ (Å) | 9.5442(35) | 9.527(10) | 9.525(5) | 9.5651(4) |
| $b$ (Å) | 11.1364(30) | 11.058(15) | 11.059(6) | 11.1284(6) |
| $c$ (Å) | 5.6286(15) | 5.615(7) | 5.603(3) | 5.6453(2) |
| $x_R$ | 0.2682(17) | 0.2815(21) | 0.2706(19) | 0.2632(2) |
| $y_R$ | 0.3729(22) | 0.3805(34) | 0.3737(24) | 0.3691(2) |
| $x_{Ni1}$ | 0.1148(7) | 0.1082(25) | 0.1155(9) | 0.1123(3) |
| $y_{Ni1}$ | 0.1390(12) | 0.1552(42) | 0.1382(16) | 0.1342(3) |
| $x_{Si1}$ | 0.3467(16) | 0.3492(56) | 0.3489(20) | 0.3475(7) |
| $y_{Si1}$ | 0.1308(35) | 0.1614(101) | 0.1258(55) | 0.1074(5) |
| $y_{Si2}$ | 0.2608(27) | 0.2056(88) | 0.2599(40) | 0.2663(5) |
| $R$ (%) | 5.1 | 9.5 | 5.5 | |

The analysis of the nuclear intensities in the neutron diffraction patterns above $T_N$ clearly shows that the samples are isostructural with the compound $Y_2Ni_3Si_5$ [10]. The crystal structure parameters determined for all three samples are given in table 2. They are compared to those obtained from x-ray diffraction in the case of an $Y_2Ni_3Si_5$ single crystal [10].
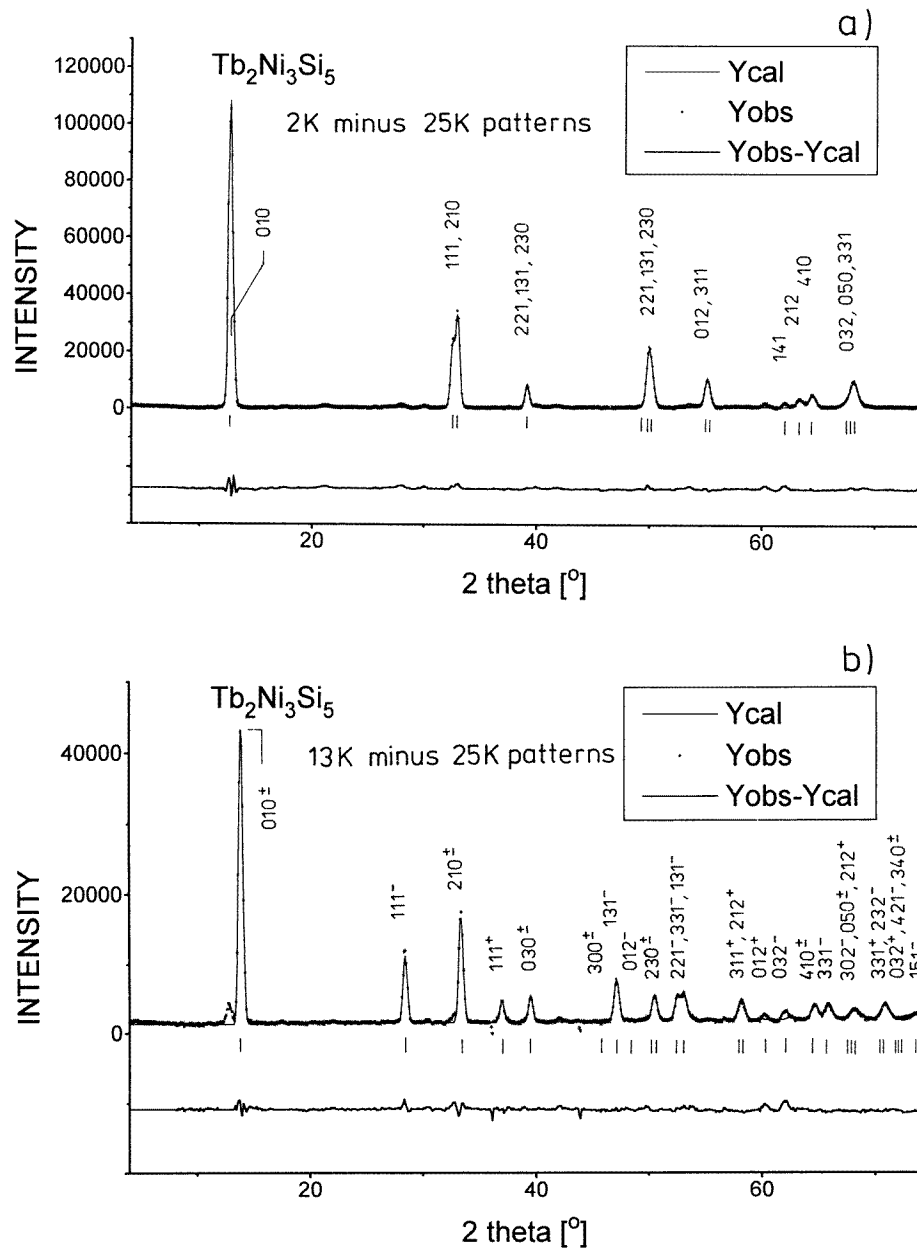
**Figure 1.** Neutron diffraction difference patterns for $Tb_2Ni_3Si_5$: (a) the difference between data taken at 2 and 25 K; and (b) the difference between data taken 13 and 25 K. The lower graph in each case shows the difference between the observed magnetic intensity and that calculated for the model structure described in the text.

## 3.2. Magnetic structure

The powder neutron diffraction patterns of $Tb_2Ni_3Si_5$ were measured at $T = 2$, 13, and 25 K (2.5 hours each). Additional measurements with a temperature step $a \approx 0.35$ K
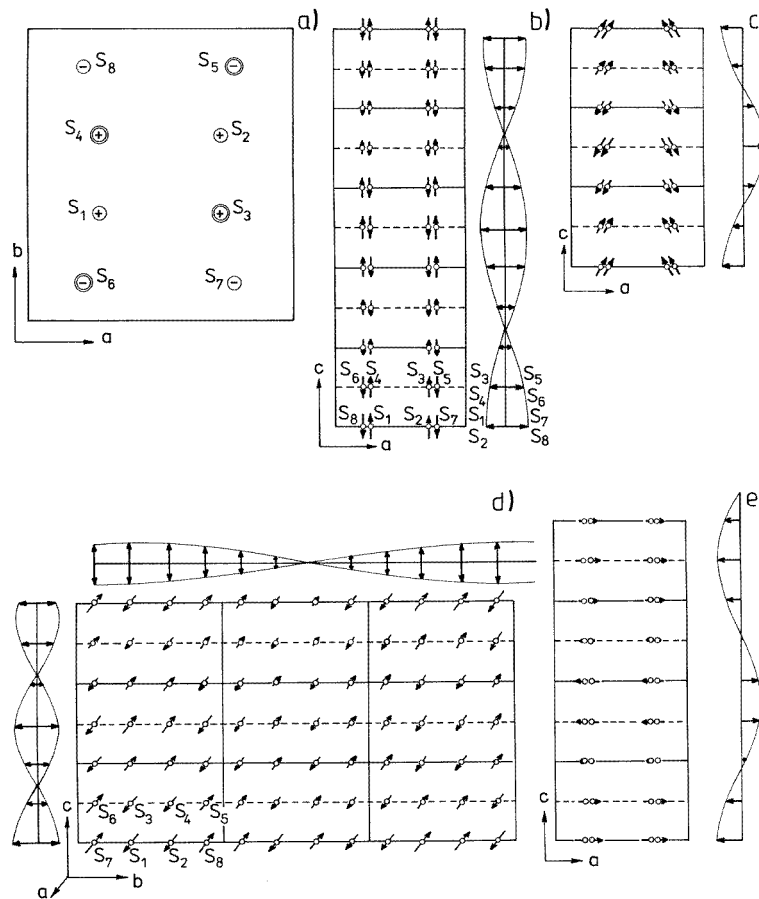
**Figure 2.** The projection of the magnetic structures of the measured compounds on different planes: (a) a collinear structure of the compound $Tb_2Ni_3Si_5$ at $T = 2$ K in the $a$–$b$ plane (the $+$ and $-$ indicate alignment parallel and antiparallel to the $c$-axis, respectively; the two sublattices ($z = 0$ and $z = 1/2$) are labelled with different sizes of circles as symbols for the atoms); (b) a sine-modulated structure of the high-temperature phase of $Tb_2Ni_3Si_5$ on the $a$–$c$ plane; (c) a sine-modulated structure measured at low temperatures on the $a$–$c$ plane for the compound $Dy_2Ni_3Si_5$; (d) a sine-modulated structure measured at high temperatures on the $b$–$c$ plane for the compound $Dy_2Ni_3Si_5$; and (e) a sine-modulated structure of $Ho_2Ni_3Si_5$ on the $a$–$c$ plane measured at 2 K.

were performed between 7.5 and 21.5 K. Figure 1 shows the neutron diffraction difference patterns of $Tb_2Ni_3Si_5$ for (a) data taken at 2 and 25 K and (b) data taken at 13 and 25 K. The observed magnetic peaks at $T = 2$ K (see figure 1(a)) can be indexed as a commensurate structure with a propagation vector along the $b$-axis, $k = (0, 1, 0)$. The magnetic moments localized on the $Tb^{3+}$ ions are situated in the following positions in the crystal unit cell: $S_1$: $(x, y, 0)$; $S_2$: $(\bar{x}, \bar{y}, 0)$; $S_3$: $(\bar{x}, y, 1/2)$; $S_4$: $(x, \bar{y}, 1/2)$; $S_5$: $(1/2 + x, 1/2 + y, 1/2)$; $S_6$: $(1/2 - x, 1/2 - y, 1/2)$; $S_7$: $(1/2 - x, 1/2 + y, 0)$; and $S_8$: $(1/2 + x, 1/2 - y, 0)$. The analysis of magnetic intensities indicates a collinear antiferromagnetic structure (see figure 2(a)) with magnetic moments equal to 7.87(4) $\mu_B$ and parallel to the $c$-axis. The disagreement factor of the magnetic intensities was $R = 1.2\%$. In this structure, the first four atoms are coupled together ferromagnetically and antiferromagnetically with four others.
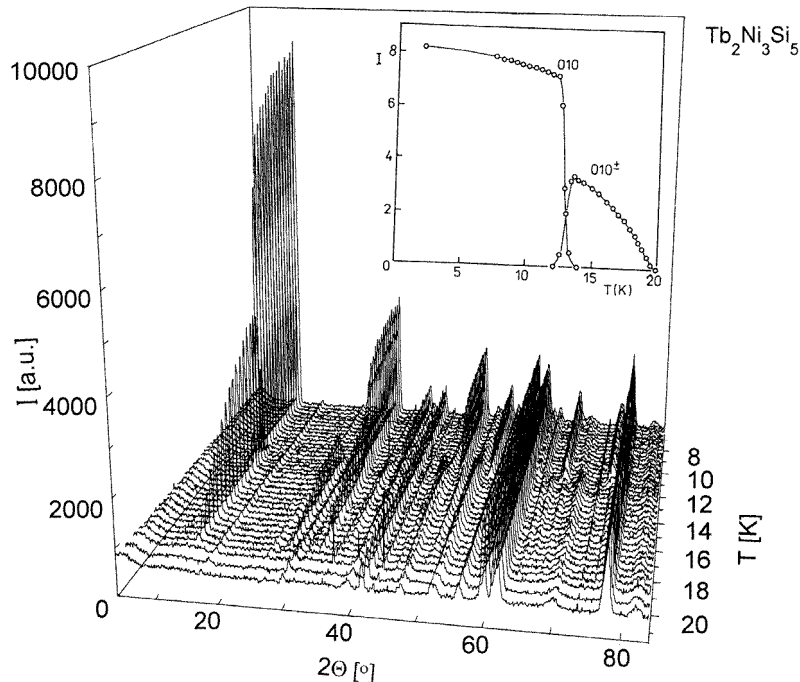
**Figure 3.** The temperature dependence of the $Tb_2Ni_3Si_5$ diffraction patterns taken in the temperature range 7.5 to 21.5 K. The angular range was from $4°$ to $84°$ ($2\theta$), and $\lambda = 2.486$ Å. The inset shows the integrated intensities of the 010 and $010^{\pm}$ reflections.

The diffraction patterns in a $2\theta$-range from 4 to $84°$ and for temperatures from 7.5 to 21.5 K are presented in figure 3. A strong change in the intensities of the magnetic peaks near $T_\tau = 13$ K is clearly visible.

The analysis of the magnetic peak intensities in the temperature region 2–12 K gives a magnetic structure similar to that observed at 2 K.

The magnetic peaks of the neutron diffraction pattern measured at $T = 13$ K (see figure 1(b)) are indexed with a wavevector $k = (0, 1.0, 0.206(1))$. The best agreement between the observed and calculated magnetic intensities ($R_{mag} = 9.1\%$) is obtained for a magnetic structure represented by the spin wave schematically displayed in figure 2(b). The magnetic moment distribution is described by $gJ \cos(2\pi k \cdot r)$, where $gJ$ is the maximum ordered moment per $Tb^{3+}$ ion, amounting to 6.55(5) $\mu_B$, and $r$ is the real-space distance. The magnetic moments are aligned along the $c$-axis.

The temperature dependence of the intensity of the magnetic peaks 010 and $010^{\pm}$ (see the inset in figure 3) indicates the Néel point to be at 19.5 K.

A careful analysis of the $Dy_2Ni_3Si_5$ magnetic data (see figure 4 in reference [5]) shows the Néel temperature to be $T_N = 9.5$ K, and an additional phase transition near $T_\tau = 4$ K. Diffraction patterns for $Dy_2Ni_3Si_5$ were measured at 2 K, 5.5 K, and 15 K, only. Magnetic contributions in the neutron pattern at 2 and 5.5 K are presented in figure 4.

The neutron diffraction pattern at $T = 2$ K is indexed with a propagation vector $k = (0, 0, 0.330(1))$, whereas that obtained at $T = 5.5$ K is indexed with $k = (0, 0.159(8), 0.356(2))$. An analysis of the neutron diffraction data indicates that at both temperatures the modulated magnetic structures are observed ($R_{mag}$ is equal to 10.4% at
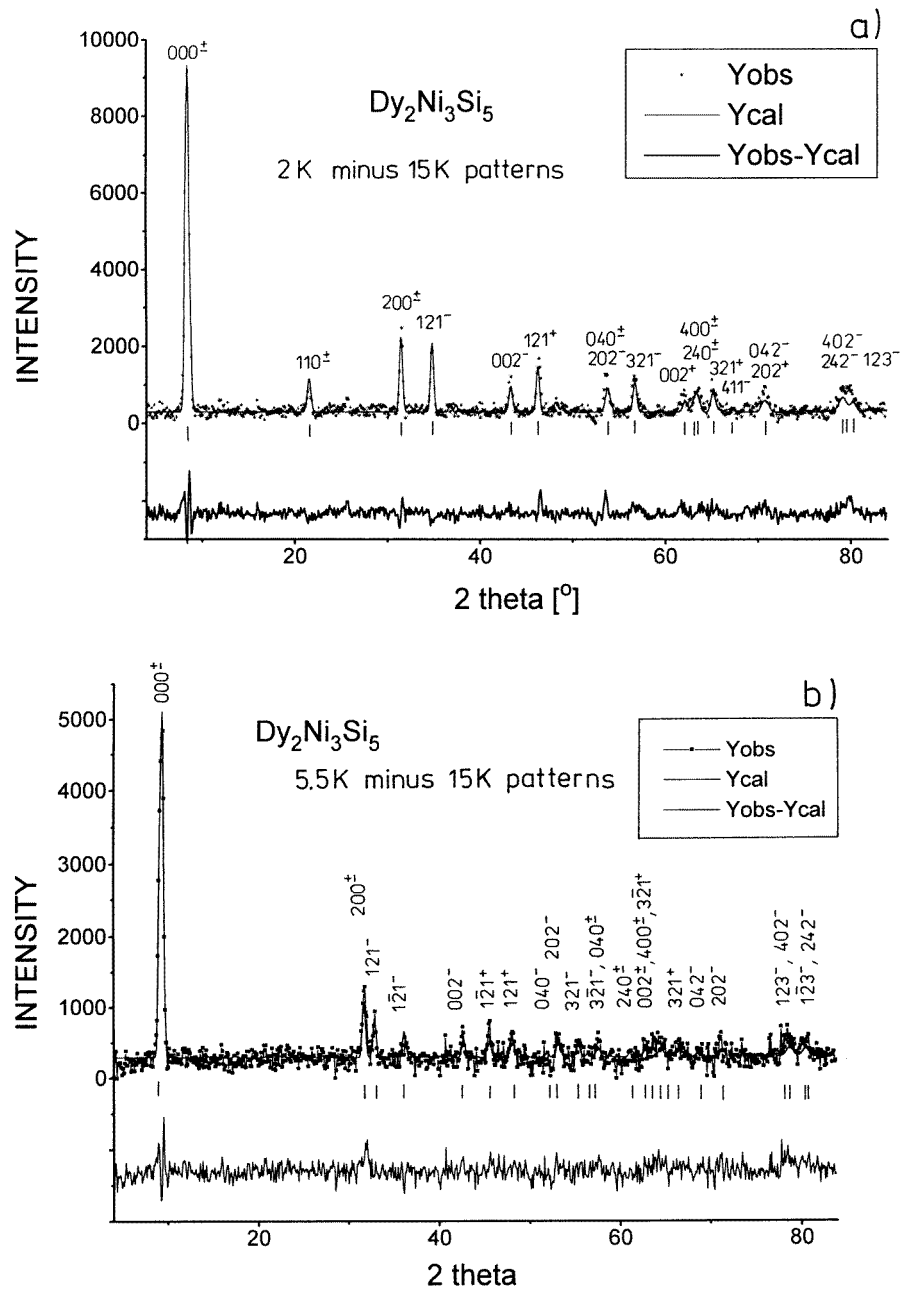
**Figure 4.** Neutron diffraction difference patterns for $Dy_2Ni_3Si_5$: (a) the difference between data taken at 2 and 15 K; and (b) the difference between data taken at 5.5 and 15 K.

2 K and 11.8% at 5.5 K). The magnetic moments of Dy atoms are equal to 7.6(1) $\mu_B$ at $T = 2$ K and 5.0(1) $\mu_B$ at 5.5 K. At $T = 5.5$ K, the magnetic moment is parallel to the $a$-axis, whereas at $T = 2$ K it lies in the $a$–$c$ plane and forms angles of 59° (for $S_1$, $S_4$, $S_6$, and $S_8$) and −59° (for $S_2$, $S_3$, $S_5$, and $S_7$) with the $c$-axis. The magnetic structures
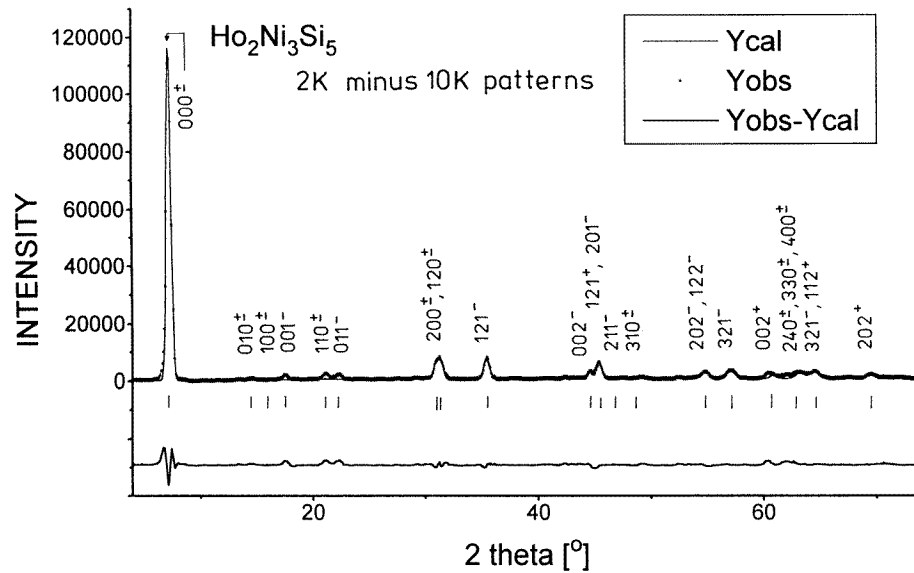
**Figure 5.** A neutron diffraction difference pattern: the difference between data taken at 2 and 10 K for $Ho_2Ni_3Si_5$. The peak at $2\theta = 17.35°$ corresponds to another unidentified phase, as it has a different temperature dependence (see figure 6).

determined are presented in figures 2(c) and 2(d).

The neutron diffraction pattern of $Ho_2Ni_3Si_5$ taken at $T = 2$ K (see figure 5) is indexed with a wavevector $k = (0, 0, 0.2855(9))$. The best agreement between the observed and calculated magnetic intensities ($R_{mag} = 2.8\%$) is obtained for a sine-modulated structure with a magnetic moment on the $Ho^{3+}$ ion equal to 7.90(5) $\mu_B$. The moments are aligned along the $a$-axis of the unit cell. The magnetic structure of $Ho_2Ni_3Si_5$ is displayed in figure 2(e).

The strong reflection $000^\pm$ monotonically decreases with increasing temperature. This indicates that the magnetic structure does not change with the temperature. The Néel temperature is 7.2 K (see figure 6).

## 4. Symmetry analysis

The experimental results obtained were analysed by means of group-theory calculations, including the symmetry analysis method [11]. This method allows one to present all magnetic structure models which could fit to the experimental data. Results of such calculations for the compounds investigated are given below.

The magnetic representation for the *Ibam* symmetry group (No 72 [12]) and 8j positions of the rare-earth atoms with $k = (0, 0, 0)$ can be presented as a direct sum of four real irreducible representations. The calculated magnetic modes are given in table 3. The magnetic structure observed at low temperatures corresponds to the $\tau_7$-representation.

The representations for the wavevector $k = (0, 0, k_z)$ are presented in table 4. The observed magnetic structure is a linear combination of $\tau_2$-basic vectors belonging to $k_1$ and $k_2 = -k_1$, with order parameter $p = (w, -we^{-\pi k_z})$.
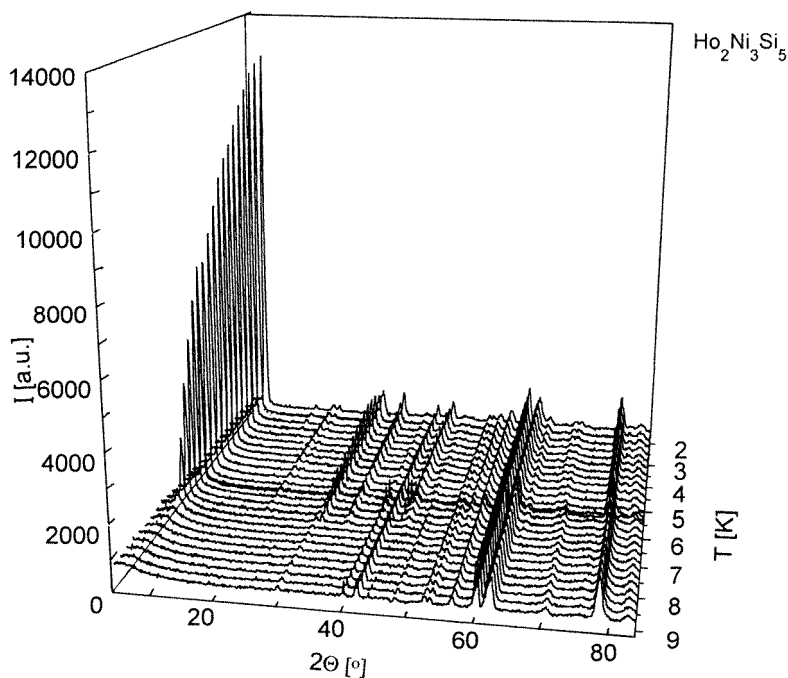
**Figure 6.** The temperature dependence of the Ho$_2$Ni$_3$Si$_5$ neutron diffraction patterns measured in the temperature range between 2 and 8.5 K. The angular range was from 4 to 84° (2$\theta$).

**Table 3.** Modes belonging to the $\tau_1$-, $\tau_4$-, $\tau_6$-, and $\tau_7$-representations of the *Ibam* (D$_{2h}^{26}$) group with the wavevector $k = (0, 0, 0)$ and the 8j position.

| Positions of the rare-earth atoms | $S_1$ | $S_2$ | $S_3$ | $S_4$ | $S_5$ | $S_6$ | $S_7$ | $S_8$ |
|---|---|---|---|---|---|---|---|---|
| $\tau_1$ | 001 | 001 | 00$\bar{1}$ | 00$\bar{1}$ | 00$\bar{1}$ | 00$\bar{1}$ | 001 | 001 |
| $\tau_4$ | 00$\bar{1}$ | 00$\bar{1}$ | 001 | 001 | 001 | 001 | 00$\bar{1}$ | 00$\bar{1}$ |
| $\tau_6$ | 001 | 00$\bar{1}$ | 00$\bar{1}$ | 001 | 00$\bar{1}$ | 001 | 001 | 00$\bar{1}$ |
| $\tau_7$ | 001 | 001 | 001 | 001 | 00$\bar{1}$ | 00$\bar{1}$ | 00$\bar{1}$ | 00$\bar{1}$ |

The moments are then as follows:

$$S_{1+t} = 2we_z \cos(k \cdot t)$$
$$S_{2+t} = 2we_z \cos(k \cdot t)$$
$$S_{3+t} = 2we_z \cos(\pi k_z + k \cdot t)$$
$$S_{4+t} = 2we_z \cos(\pi k_z + k \cdot t)$$
$$S_{5+t} = 2we_z \cos(\pi k_z + k \cdot t)$$
$$S_{6+t} = 2we_z \cos(\pi k_z + k \cdot t)$$
$$S_{7+t} = 2we_z \cos(k \cdot t)$$
$$S_{8+t} = 2we_z \cos(k \cdot t).$$

**Table 4.** Modes belonging to the $\tau_1$-, $\tau_2$-, $\tau_3$-, and $\tau_4$-representations of the *Ibam* ($D_{2h}^{26}$) group with the wavevector $\mathbf{k} = (0, 0, k_z)$ and the 8j position. $\alpha = e^{i\pi k_z}$.

| Positions of atoms | 1 | 2 | 3 | 4 | 5 | 6 | 7 | 8 |
|---|---|---|---|---|---|---|---|---|
| $\mathbf{k}_1$ | | | | | | | | |
| $\tau_1$ | 100 | $\bar{1}00$ | $\alpha00$ | $\bar{\alpha}00$ | $\alpha00$ | $\bar{\alpha}00$ | 100 | $\bar{1}00$ |
| | 010 | $0\bar{1}0$ | $0\bar{\alpha}0$ | $0\alpha0$ | $0\alpha0$ | $0\bar{\alpha}0$ | $0\bar{1}0$ | 010 |
| | 001 | 001 | $00\bar{\alpha}$ | $00\bar{\alpha}$ | $00\alpha$ | $00\alpha$ | $00\bar{1}$ | $00\bar{1}$ |
| $\tau_2$ | 100 | $\bar{1}00$ | $\bar{\alpha}00$ | $\alpha00$ | $\alpha00$ | $\bar{\alpha}00$ | $\bar{1}00$ | 100 |
| | 010 | $0\bar{1}0$ | $0\bar{\alpha}0$ | $0\bar{\alpha}0$ | $0\alpha0$ | $0\bar{\alpha}0$ | 010 | $0\bar{1}0$ |
| | 001 | 001 | $00\alpha$ | $00\alpha$ | $00\alpha$ | $00\alpha$ | 001 | 001 |
| $\tau_3$ | 100 | 100 | $\alpha00$ | $\alpha00$ | $\alpha00$ | $\alpha00$ | 100 | 100 |
| | 010 | 010 | $0\bar{\alpha}0$ | $0\bar{\alpha}0$ | $0\alpha0$ | $0\alpha0$ | $0\bar{1}0$ | $0\bar{1}0$ |
| | 001 | $00\bar{1}$ | $00\bar{\alpha}$ | $00\alpha$ | $00\alpha$ | $00\bar{\alpha}$ | $00\bar{1}$ | 001 |
| $\tau_4$ | 100 | 100 | $\bar{\alpha}00$ | $\bar{\alpha}00$ | $\alpha00$ | $\alpha00$ | $\bar{1}00$ | $\bar{1}00$ |
| | 010 | 010 | $0\alpha0$ | $0\alpha0$ | $0\alpha0$ | $0\alpha0$ | 010 | 010 |
| | 001 | $00\bar{1}$ | $00\alpha$ | $00\bar{\alpha}$ | $00\alpha$ | $00\bar{\alpha}$ | 001 | $00\bar{1}$ |
| $\mathbf{k}_2 = -\mathbf{k}_1$ | | | | | | | | |
| $\tau_1$ | $\alpha00$ | $\alpha00$ | $\bar{1}00$ | 100 | $\bar{1}00$ | 100 | $\bar{\alpha}00$ | $\alpha00$ |
| | $0\bar{\alpha}0$ | $0\alpha0$ | 010 | $0\bar{1}0$ | $0\bar{1}0$ | 010 | $0\bar{\alpha}0$ | $0\bar{\alpha}0$ |
| | $00\alpha$ | $00\alpha$ | $00\bar{1}$ | $00\bar{1}$ | 001 | 001 | $00\bar{\alpha}$ | $00\bar{\alpha}$ |
| $\tau_2$ | $\alpha00$ | $\bar{\alpha}00$ | $\bar{1}00$ | 100 | 100 | $\bar{1}00$ | $\bar{\alpha}00$ | $\alpha00$ |
| | $0\alpha0$ | $0\bar{\alpha}0$ | 010 | $0\bar{1}0$ | 010 | $0\bar{1}0$ | $0\alpha0$ | $0\bar{\alpha}0$ |
| | $00\bar{\alpha}$ | $00\bar{\alpha}$ | $00\bar{1}$ | $00\bar{1}$ | $00\bar{1}$ | $00\bar{1}$ | $00\alpha$ | $00\alpha$ |
| $\tau_3$ | $\alpha00$ | $\alpha00$ | 100 | 100 | 100 | 100 | $\alpha00$ | $\alpha00$ |
| | $0\alpha0$ | $0\alpha0$ | $0\bar{1}0$ | $0\bar{1}0$ | 010 | 010 | $0\alpha0$ | $0\bar{\alpha}0$ |
| | $00\alpha$ | $00\alpha$ | 001 | $00\bar{1}$ | $00\bar{1}$ | 001 | $00\alpha$ | $00\bar{\alpha}$ |
| $\tau_4$ | $\bar{\alpha}00$ | $\bar{\alpha}00$ | 100 | 100 | $\bar{1}00$ | $\bar{1}00$ | $\alpha00$ | $\alpha00$ |
| | $0\bar{\alpha}0$ | $0\bar{\alpha}0$ | $0\bar{1}0$ | $0\bar{1}0$ | $0\bar{1}0$ | $0\bar{1}0$ | $0\bar{\alpha}0$ | $0\bar{\alpha}0$ |
| | $00\alpha$ | $00\bar{\alpha}$ | $00\bar{1}$ | 001 | 001 | $00\bar{1}$ | $00\alpha$ | $00\bar{\alpha}$ |

The magnetic structure of $Dy_2Ni_3Si_5$ at low temperatures, with the Dy magnetic moment in the $a$–$c$ plane (see figure 2(c)) is represented by

$$S_{1,8+t} = 2(u e_x + w e_z)\cos(\mathbf{k} \cdot \mathbf{t})$$
$$S_{2,7+t} = 2(-u e_x + w e_z)\cos(\mathbf{k} \cdot \mathbf{t})$$
$$S_{4,5+t} = 2(u e_x + w e_z)\cos(\pi k_z + \mathbf{k} \cdot \mathbf{t})$$
$$S_{3,6+t} = 2(-u e_x + w e_z)\cos(\pi k_z + \mathbf{k} \cdot \mathbf{t})$$

where $u$ and $w$ are the components of the order parameters $p_1 = (u; u e^{-i\pi k_z})$ and $p_2 = (w; -w e^{-i\pi k_z})$.

$Ho_2Ni_3Si_5$ has a magnetic structure similar to that of $Dy_2Ni_3Si_5$ at low temperature, with the magnetic moment parallel to the $a$-axis (see figure 2(e)). The high-temperature magnetic structures of $Tb_2Ni_3Si_5$ and $Dy_2Ni_3Si_5$ are described by the two-component wavevector $\mathbf{k} = (0, k_y, k_z)$. The calculated magnetic modes are presented in table 5. The possible magnetic structures are as follows.

(i) When the magnetic moment is parallel to the $c$-axis, then the representation $\tau_2$ with

**Table 5.** Modes belonging to the $\tau_1$- and $\tau_2$-representations of the *Ibam* ($D_{2h}^{26}$) group with the wavevector $\boldsymbol{k} = (0, k_y, k_z)$ and the 8j positions. (In the last column, 1O stands for 'One orbital' and 2O stands for 'Two orbitals'.)

| Positions of atoms | 1 | 2 | 3 | 4 | 5 | 6 | 7 | 8 | |
|---|---|---|---|---|---|---|---|---|---|
| (a) The sequence of signs | | | | | | | | | |
| $k_1$ | 100 | | 100 | | 100 | | 100 | | 1O |
| | 010 | | 0$\bar{1}$0 | | 010 | | 0$\bar{1}$0 | | |
| | 001 | | 00$\bar{1}$ | | 001 | | 00$\bar{1}$ | | |
| $\tau_1$ | | 100 | | 100 | | 100 | | 100 | 2O |
| | | 0$\bar{1}$0 | | 010 | | 0$\bar{1}$0 | | 010 | |
| | | 00$\bar{1}$ | | 001 | | 00$\bar{1}$ | | 001 | |
| $k_2 = -k_1$ | | 100 | | 100 | | 100 | | 100 | 1O |
| | | 010 | | 0$\bar{1}$0 | | 010 | | 0$\bar{1}$0 | |
| | | 001 | | 00$\bar{1}$ | | 001 | | 00$\bar{1}$ | |
| $\tau_1$ | 100 | | 100 | | 100 | | 100 | | 2O |
| | 0$\bar{1}$0 | | 010 | | 0$\bar{1}$0 | | 010 | | |
| | 00$\bar{1}$ | | 001 | | 00$\bar{1}$ | | 001 | | |
| $k_1$ | 100 | | $\bar{1}$00 | | 100 | | $\bar{1}$00 | | 1O |
| | 010 | | 010 | | 010 | | 010 | | |
| | 001 | | 001 | | 001 | | 001 | | |
| $\tau_2$ | | $\bar{1}$00 | | 100 | | $\bar{1}$00 | | 100 | 2O |
| | | $\bar{1}$00 | | 010 | | 010 | | 010 | |
| | | 001 | | 001 | | 001 | | 001 | |
| $k_2 = -k_1$ | | $\bar{1}$00 | | 100 | | $\bar{1}$00 | | 100 | 1O |
| | | 0$\bar{1}$0 | | 0$\bar{1}$0 | | 0$\bar{1}$0 | | 0$\bar{1}$0 | |
| | | 00$\bar{1}$ | | 00$\bar{1}$ | | 00$\bar{1}$ | | 00$\bar{1}$ | |
| $\tau_2$ | 100 | | $\bar{1}$00 | | 100 | | $\bar{1}$00 | | 2O |
| | 0$\bar{1}$0 | | 0$\bar{1}$0 | | 0$\bar{1}$0 | | 0$\bar{1}$0 | | |
| | 00$\bar{1}$ | | 00$\bar{1}$ | | 00$\bar{1}$ | | 00$\bar{1}$ | | |
| (b) The phase factors | | | | | | | | | |
| $k_1$ | 1 | | $e^{-i\pi k_z}$ | | $e^{i\pi(k_y+k_z)}$ | | $e^{-i\pi k_y}$ | | 1O |
| $\tau_1$ | | $e^{i 2\pi k_z}$ | | 1 | | $e^{i\pi k_y}$ | | $e^{i\pi(k_y+k_z)}$ | 2O |
| $k_2$ | | $e^{-i\pi(2k_{2y}+k_z)}$ | | $e^{-i 2\pi k_{2y}}$ | | $e^{i\pi(2k_y+k_y)}$ | | $e^{i\pi(k_y+2k_{2y}+k_z)}$ | 1O |
| $= -k_1$ | $e^{-i 2\pi k_{2y}}$ | | $e^{-i\pi(2k_y-k_z)}$ | | $e^{i\pi(k_y-2k_{2y}+k_z)}$ | | $e^{i\pi(k_y-2k_y)}$ | | 2O |
| $k_1$ | 1 | | $e^{i\pi k_z}$ | | $e^{i\pi(k_y+k_z)}$ | | $e^{i\pi k_y}$ | | 1O |
| $\tau_2$ | | $e^{-i 2\pi k_z}$ | | 1 | | $e^{-i\pi k_y}$ | | $e^{-i\pi(k_y+k_z)}$ | 2O |
| $k_2$ | | $e^{i\pi(2k_y+k_z)}$ | | $e^{i 2\pi k_{2y}}$ | | $e^{i\pi(k_y+2k_{2y})}$ | | $e^{i\pi(k_y+2k_{2y}+k_z)}$ | 1O |
| $= -k_1$ | $e^{i 2\pi k_y}$ | | $e^{i\pi(k_{2y}-k_z)}$ | | $e^{-i\pi(k_y-2k_{2y}+k_z)}$ | | | | 2O |

the order parameter $p_1 = (w, -we^{i 2\pi k_y})$ gives

$$\boldsymbol{S}_{1+t} = 2w\boldsymbol{e}_z \cos \boldsymbol{k} \cdot \boldsymbol{t} \qquad \boldsymbol{S}_{5+t} = 2w\boldsymbol{e}_z \cos(\boldsymbol{k} \cdot \boldsymbol{t} + \pi k_z + \pi k_y)$$

$$\boldsymbol{S}_{2+t} = 2w\boldsymbol{e}_z \cos(\boldsymbol{k} \cdot \boldsymbol{t} + \varphi) \qquad \boldsymbol{S}_{6+t} = 2w\boldsymbol{e}_z \cos(\boldsymbol{k} \cdot \boldsymbol{t} - \pi k_y - \pi k_z + \varphi)$$

$$\boldsymbol{S}_{3+t} = 2w\boldsymbol{e}_z \cos(\boldsymbol{k} \cdot \boldsymbol{t} + \pi k_z) \qquad \boldsymbol{S}_{7+t} = 2w\boldsymbol{e}_z \cos(\boldsymbol{k} \cdot \boldsymbol{t} + \pi k_y)$$

$$\boldsymbol{S}_{4+t} = 2w\boldsymbol{e}_z \cos(\boldsymbol{k} \cdot \boldsymbol{t} - \pi k_z + \varphi) \qquad \boldsymbol{S}_{8+t} = 2w\boldsymbol{e}_z \cos(\boldsymbol{k} \cdot \boldsymbol{t} - \pi k_y + \varphi).$$

(ii) When the magnetic moment is parallel to the *a*-axis, then the representation $\tau_1$ with the order parameter $p = (u, ue^{2\pi ik_y})$ gives

$$S_{1+t} = 2ue_x \cos k \cdot t \qquad\qquad S_{5+t} = 2ue_x \cos(k \cdot t + \pi k_z + \pi k_y)$$

$$S_{2+t} = 2ue_x \cos(k \cdot t + \varphi) \qquad\qquad S_{6+t} = 2ue_x \cos(k \cdot t - \pi k_y - \pi k_z + \varphi)$$

$$S_{3+t} = 2ue_x \cos(k \cdot t + \pi k_z) \qquad\qquad S_{7+t} = 2ue_x \cos(k \cdot t + \pi k_y)$$

$$S_{4+t} = 2ue_x \cos(k \cdot t - \pi k_z + \varphi) \qquad\qquad S_{8+t} = 2ue_x \cos(k \cdot t - \pi k_y + \varphi)$$

where $\varphi$ is the phase shift.

The magnetic structure of $Tb_2Ni_3Si_5$ at high temperatures is described by the $\tau_2$-representation, whereas for $Dy_2Ni_3Si_5$ at high temperatures it is described by the $\tau_1$-representation.

## 5. Discussion

In the ternary rare-earth compounds investigated in this work, the magnetic moments are localized on the rare-earth atoms only. In $R_2Ni_3Si_5$ compounds as in $RNi_2X_2$ compounds [1, 13], the Ni atoms have no magnetic moment.

The neutron diffraction data presented in this work indicate that the magnetic structures change with increasing temperature.

The magnetic structure of $Tb_2Ni_3Si_5$ commensurate with the crystal unit cell below 13 K becomes incommensurate above this temperature.

In $Dy_2Ni_3Si_5$, one incommensurate structure transforms into another one with the change of the direction of the magnetic moments with increasing temperature.

A transition between two magnetic phases is observed in many lanthanide intermetallic compounds [14, 15]. The $Ho_2Ni_3Si_5$ compound has only one incommensurate phase in the temperature range around 2 K and where $T_N = 7.2$ K.

In $R_2Ni_3Si_5$ compounds, the interatomic distances between the rare-earth atoms are large [10]. The large interatomic distance and an oscillatory character of the magnetic ordering scheme observed for all three compounds suggest that the well-known Ruderman–Kittel–Kasuya–Yosida (RKKY) theory can be used to explain the stability of the magnetic structure. In this model the critical temperature of the magnetic ordering ($T_C$, $T_N$) is proportional to the de Gennes factor $(g_J - 1)J(J + 1)$. This relation for $R_2Ni_3Si_5$ compounds is presented in figure 7. According to the de Gennes scaling in the isostructural series, $T_N$ should be highest for the Gd-containing compounds. For the compounds discussed, the maximum is observed for Tb-containing compounds. The shifting of $T_N$ for Tb, and a large difference between the observed and calculated values of $T_N$ for light rare-earth compounds can result from the crystalline-electric-field (CEF) effect. The phenomenon of the shift of $T_N$ for heavy rare-earth compounds caused by the crystal electric field was discussed by Noakes and Shenoy [16]. The following formula describes the Néel temperature:

$$T_N = 2J_{ex}(g_J - 1)^2 \sum J_z^2 \exp(-3B_2^0 J_z^2 / T_N) \left\{ \sum \exp(-3B_2^0 J_z^2 / T_N) \right\}^{-1} \tag{1}$$

where $J_{ex}$ is the exchange constant for the 4f atoms, and $B_2^0$ is a crystal-field parameter. Since $Gd^{3+}$ is an S-state ion which is not influenced by the crystal electric field, its value of $T_N$ can be used to fix the value of the exchange constant $J_{ex} = 2.85$ K. Numerical calculation of the Néel temperature according to equation (1) for other heavy rare-earth ions gives a good agreement with the experimental data. A simple $B_2^0$-term produces the maximum in $T_N$ for Tb compounds. A large disagreement between the calculated and
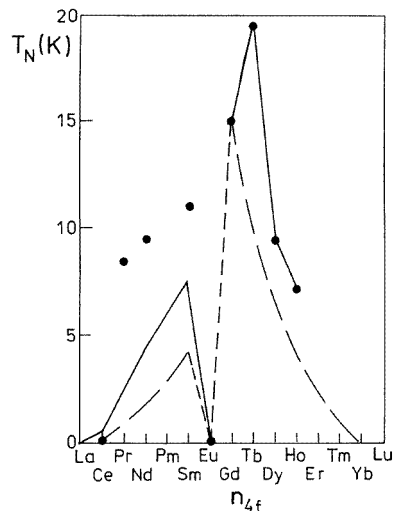
**Figure 7.** Magnetic transition temperatures of $R_2Ni_3Si_5$ compounds plotted against the number of 4f electrons. A solid line displays the influence of the crystal field on the $T_N$-function versus the number of 4f electrons. The broken line represents the de Gennes function normalized with respect to $Gd_2Ni_3Si_5$.

observed values of $T_N$ for light rare-earth compounds is observed (see figure 7). Similar discrepancies between the observed and calculated values of the Néel temperature have been observed for a large number of the rare-earth intermetallic compounds. See, for example, the data for $RGa_2$ compounds (figure 1 in reference [17]), where the experimental values are well above the theoretical ones. The fact that experimental values of the Néel temperature are larger than the theoretical ones calculated using the Hamiltonian for the compounds with exchange interactions of RKKY type and experiencing crystal-electric-field effects implies that the other interaction influences the magnetic interactions. The local coupling between the 4f shell and the conduction electrons is much stronger than expected, perhaps due to a large orbital contribution to the exchange coupling [18]. It is also possible that the strengthening of the local coupling due to the large spatial extent of the 4f shell for the light rare earths leads to a large overlap of the 4f and 5d orbitals [19].

The partial quenching of the magnetic moment of rare-earth atoms in an ordered state compared to the free $R^{3+}$-ion values also indicates an influence of the CEF on the magnetic properties of $R_2Ni_3Si_5$ compounds.

The $R_2Ni_3Si_5$ compounds crystallize in the orthorhombic $U_2Co_3Si_5$-type crystal structure, which is an orthorhombic superstructure of the tetragonal $ThCr_2Si_2$ ($CeAl_2Ge_2$) type [6]. The unit-cell volume of a $U_2Co_3Si_5$-type structure is four times larger than the volume of the corresponding $ThCr_2Si_2$-type structure ($a \approx c_{ThCr_2Si_2}$, $b \approx 2\sqrt{2}\,a_{ThCr_2Si_2}$, and $c \approx \sqrt{2}\,a_{ThCr_2Si_2}$). The magnetic structures of $TbNi_2Si_2$ and $DyNi_2Si_2$ change with increasing temperature. For $TbNi_2Si_2$ below $T_\tau = 9$ K, a collinear antiferromagnetic structure is observed that turns into an incommensurate one above $T_\tau$ [13]. In the case of $DyNi_2Si_2$ below $T_\tau = 3.7$ K, the magnetic structure is of the square-wave type, whereas above $T_\tau$ it transforms into an amplitude-modulated sine-wave-type structure [20]. For both phases of these compounds, the magnetic moment is parallel to the $c$-axis.

For many intermetallic compounds [14], the direction of the magnetic moments changes with the change in the f-electron number. Such a phenomenon is also observed in $R_2Ni_3Si_5$

(R = Tb, Dy, Ho) compounds.

The results of this work indicate a change in the direction of the magnetic moment with an increase in the number of 4f electrons of rare-earth atoms, and with increasing temperature. In both phases of $Tb_2Ni_3Si_5$, the magnetic moments are parallel to the $c$-axis, corresponding to the short lattice constant. For $Dy_2Ni_3Si_5$ in the low-temperature phase, the magnetic moment forms an angle with the $c$-axis, while in the high-temperature phase, it is parallel to the $a$-axis. The magnetic moment for $Ho_2Ni_3Si_5$ is parallel to the $a$-axis.

The fact that the orientation of magnetic moments in $R_2Ni_3Si_5$ is different from that in $RNi_2Si_2$ suggests that the surrounding local atoms have a large influence on the crystal field, which causes anisotropy.

## Acknowledgments

## References

[1] Szytuła A and Leciejewicz J 1994 *Handbook of Crystal Structures and Magnetic Properties of Rare Earth Intermetallics* (Boca Raton, FL: Chemical Rubber Company Press)
[2] Bodak O I, Kotur B Ya, Yarovets VI and Gladyshevskii E I 1977 *Sov. Phys.–Crystallogr.* **22** 217
[3] Mazumdar C, Nagarajan R, Gupta L C, Vijayaraghavan R, Godart G and Padalia B P 1994 *J. Appl. Phys.* **75** 7155
[4] Mazumdar C, Nagarajan R, Gupta L C, Vijayaraghavan R, Godart G and Padalia B P 1994 *IEEE Trans. Magn.* **30** 4960
[5] Mazumdar C, Nagarajan R, Gupta L C, Padalia B D and Vijayaraghavan R 1995 *J. Magn. Magn. Mater.* **140–144** 917
[6] Aksel'rud L G, Yarmoluk Ya P and Gladyshevskii E I 1977 *Sov. Phys.–Crystallogr.* **22** 492
[7] Rodriguez-Carvajal J 1993 *Physica* B **192** 55
[8] Sears V F 1992 *Neutron News* **3** 29
[9] Freeman A J and Desclaux J P 1979 *J. Magn. Magn. Mater.* **12** 11
[10] Chabot B and Parthé E 1984 *J. Less-Common Met.* **97** 285
[11] Sikora W 1994 *Workshop on Magnetic Structures and Phase Transitions (Kraków)* p 93
[12] *International Tables for X-ray Crystallography* 1952 vol I (Birmingham: Kynoch) p 164
[13] Barandiarán J M, Gignoux D, Schmitt D, Gómez Sal J C and Rodríguez Fernández J 1987 *J. Magn. Magn. Mater.* **69** 61
[14] Szytuła A 1991 *Handbook of Magnetic Materials* vol 6, ed K H J Buschow (Amsterdam: North-Holland) p 85
[15] Gignoux D and Schmitt D 1993 *Phys. Rev.* B **48** 12 682
[16] Noakes D R and Shenoy G K 1982 *Phys. Lett.* **91A** 35
[17] Ball A R, Gignoux D, Schmitt D and Zhang F Y 1995 *J. Magn. Magn. Mater* **140–144** 1121
[18] Belorizky E, Niez J J and Levy P M 1981 *Phys. Rev.* B **23** 3360
[19] Belorizky E, Gavigan J P, Givord D and Li H S 1988 *Europhys. Lett.* **5** 349
[20] Ito M, Deguchi H, Takeda K and Hashimoto Y 1994 *J. Phys. Soc. Japan* **9** 3019